

Testing the Origin of Hot Jupiters with Ariel

LINA D'AOUST ^{1,2} BEN COULL-NEVEU ³ EVE J. LEE ^{4,3,2} AND NICOLAS B. COWAN ^{3,5,2}

¹*Department of Physics & Astronomy, University of Victoria, Victoria, British Columbia, V8P 5C2, Canada*

²*Trottier Institute for Research on Exoplanets (IREx), Université de Montréal, Canada*

³*Department of Physics and Trottier Space Institute, McGill University, 3600 rue University, H3A 2T8 Montreal QC, Canada*

⁴*Department of Astronomy & Astrophysics, University of California, San Diego, La Jolla, CA 92093-0424, USA*

⁵*Department of Earth & Planetary Sciences, 3450 University Street Montreal, QC H3A 0E8, Canada*

ABSTRACT

In spite of their long detection history, the origin of hot Jupiters remains to be resolved. While multiple dynamical evidence suggests high-eccentricity migration is most likely, conflicts remain when considering hot Jupiters as a population in the context of warm and cold Jupiters. Here, we turn to atmospheric signatures as an alternative mean to test the origin theory of hot Jupiters, focusing on population level trends that arise from post-formation pollution, motivated by the upcoming Ariel space mission whose goal is to deliver a uniform sample of exoplanet atmospheric constraints. We experiment with post-formation pollution by planetesimal accretion, pebble accretion, and disk-induced migration and find that an observable signature of post-formation pollution is only possible under pebble accretion in metal-heavy disks. If most hot Jupiters arrive at their present orbit by high-eccentricity migration while warm Jupiters emerge largely in situ, we expect the atmospheric water abundance of hot Jupiters to be significantly elevated compared to warm Jupiters, at a level that is easily detectable by Ariel transit survey. We provide suggestions for future comparative atmospheric characterization between hot Jupiters and wide-orbit directly imaged planets to elucidate the properties of the dust substructures in protoplanetary disks.

1. INTRODUCTION

Hot Jupiters are one of the first kind of exoplanet ever detected. Yet, their origin remains debated. Broadly, three origin hypotheses have been proposed in the literature, including in situ formation, disk-induced migration, and high-eccentricity migration, all of which have their successes and shortcomings (see [R. I. Dawson & J. A. Johnson 2018](#), for a review). Among these three, in situ formation is the least likely given the need to coagulate cores of mass $\gtrsim 10M_{\oplus}$ (e.g., [R. R. Rafikov 2006](#); [E. J. Lee et al. 2014](#); [A.-M. a. Piso et al. 2015](#); [V. Savignac & E. J. Lee 2024](#)) which is prohibitively large at such short orbital distances (e.g., [B. Bitsch et al. 2018](#); [J. Fung & E. J. Lee 2018](#)).

Between disk-induced and high-eccentricity migration, there is growing evidence that the latter is more likely, including the distribution of obliquities and eccentricities ([C. Petrovich & S. Tremaine 2016](#); [M. Rice et al. 2022a](#)), the shape of the upper edge of the sub-Jovian desert ([T. Matsakos & A. Königl 2016](#); [J. E. Owen & D.](#)

[Lai 2018](#)), and the systematically older ages of true hot Jupiters compared to puffy sub-Neptunes ([A. Karalis et al. 2025](#)). Constructing a single theory that explains hot Jupiters in the context of warm and cold Jupiters has been challenging, however. For example, approximately half of warm Jupiters are accompanied by sub-Neptune companions ([C. Huang et al. 2016](#)), a configuration that is hard to reconcile with high-eccentricity migration scenarios, which often lead to orbital instability ([F. Antonini et al. 2016](#)). Smaller obliquities of tidally detached warm Jupiter systems further support their more dynamically quiescent origin compared to hot Jupiters (e.g., [M. Rice et al. 2022a](#); [X.-Y. Wang et al. 2024](#)). In addition, disk-induced migration can explain well the overall shape of the orbital period distribution of hot, warm and cold Jupiters but underestimates the typical mass of hot Jupiters ([T. Hallatt & E. J. Lee 2020](#)).

An alternative path to resolving the origin of hot Jupiters is to use chemical abundances. Early and recent studies have focused on the expected atmospheric composition of hot Jupiters depending on their initial formation locations (e.g., [N. Madhusudhan et al. 2014](#); [A. D. Schneider & B. Bitsch 2021](#); [A. B. T. Penzlin et al.](#)

Email: linatheresed@gmail.com, benjamin.coull-neveu@mail.mcgill.ca, evelee@ucsd.edu, nicolas.cowan@mcgill.ca

2024), based on the radial variation in chemical content in protoplanetary disks (e.g., K. I. Öberg et al. 2011; P. Mollière et al. 2022). These studies generally expect high C/O ratio as a signature of formation beyond the iceline as the water molecules are expected to be in solid form and gas giants, by definition, are mostly gas. Pollution of the envelope by continued solid accretion after formation can complicate this picture, however, as the infalling solids are expected to evaporate within the envelope (e.g., E. Vlahos et al. 2024). Support for post-formation pollution of gas giants may be found in the high atmospheric metallicities of our own Jupiter (e.g., K. I. Öberg & R. Wordsworth 2019) and HR 8799 planets (E. Nasedkin et al. 2024; Ruffio et al. submitted), as well as low C/O ratio of β Pic b (GRAVITY Collaboration et al. 2020).

While the collection of dynamical evidence suggests distinct origins of hot vs. warm Jupiters, a clear alternative test from atmospheric studies remains to be proposed. In this paper, we aim to develop population-level atmospheric signatures (i.e., trends) as a probe of disk-induced vs. high-eccentricity migration for hot and warm Jupiters. We are particularly motivated by the upcoming European Space Agency’s Ariel mission that promises to deliver a uniform sample of gas giants over a range of parameter space, ideally suited to identifying trends rather than a deep dive into individual planets.

Ariel is scheduled to launch at the end of the decade to perform a survey of exoplanet spectra (G. Tinetti et al. 2018; G. Tinetti et al. 2021). Much of Ariel’s four year primary mission will be devoted to transit spectroscopy of hundreds of diverse exoplanets—primarily gas giants (G. Tinetti et al. 2021). As outlined in the Ariel Definition Study Report (G. Tinetti et al. 2022), Ariel would perform observations of four overlapping target lists: Reconnaissance Survey (Tier 1), Deep Survey (Tier 2), Benchmark Planets (Tier 3), and Phase Curves (Tier 4). We focus on the Tier 2 survey, which is expected to make up the bulk of the Ariel transit spectroscopy.

The spectral coverage and signal-to-noise of Ariel Tier 2 transit spectra are sufficient to usefully constrain the abundance of the main oxygen- and carbon-bearing species (J. K. Barstow et al. 2022), hence providing a measurement of atmospheric metallicity (M. R. Swain et al. 2024). Tier 2 spectra have planetary signal-to-noise ratios of at least 7 at a spectral resolution of $R = 10, 50,$ and 15 in NIRSPEC, AIRS-CH0, and AIRS-CH1, respectively (L. V. Mugnai et al. 2021). Uniform observations of this quality for hundreds of exoplanets and their host stars will provide an unprecedented opportunity to test planet formation theory by quantifying trends between atmospheric metallicity, orbital and

planetary parameters (C. Danielski et al. 2022; D. Turriani et al. 2022).

Our paper is organized as follows. We outline the underlying theoretical calculations for post-formation pollution in Section 2. Resulting trends of atmospheric metallicity and water abundance with respect to orbital period are presented in Section 3. Methods and the outcomes of simulated Ariel transit survey are shown in Section 4. We discuss shortcomings, implications, and suggestions for optimal observation strategy in Section 5, and conclude in Section 6.

2. THEORIES

We first construct theoretically expected trends in atmospheric metallicity, focusing on the deviation of the planetary metallicity from the stellar value due to post-formation pollution. Our assumptions are: 1) the giants inherit the stellar metallicity at formation; and 2) the infalling material is well-mixed with the envelope by convection. Following these assumptions, we consider observable atmospheric metallicity as the mass of solids accreted divided by the mass of the planet, fixed to one Jupiter mass for simplicity.⁶

2.1. Pollution by Solid Accretion

We consider three different paths of pollution: in situ planetesimal accretion, in situ pebble accretion, and migration. In reality, the modes of accretion are likely mixed, but we keep the three paths distinct for clarity. In all cases, we consider a giant planet of mass $M_p = 1M_{\text{JUP}}$ and radius $R_p = 1R_{\text{JUP}}$ to have already formed and be simply further accreting the remaining solids in the disk.

Under planetesimal accretion, we adopt

$$\dot{M}_{\text{pla}} = \Sigma \Omega R_p^2 \quad (1)$$

where Σ is the local solid disk surface density, $\Omega \equiv \sqrt{GM_\star/a^3}$ is the Keplerian orbital frequency, G is the gravitational constant, M_\star is the mass of the star, a is the orbital distance, and R_p is the radius of the planet. We do not consider gravitational focusing as it is unclear a priori what the typical random velocity of the planetesimals should be. We therefore consider the simplest case of geometric cross section.

Next, we consider pebble accretion, whereby smaller solids that are marginally aerodynamically coupled to the gas are accreted to a planet through gas drag (e.g.,

⁶ We have implicitly assumed the mass of the initial rocky core that triggered the nucleation of a giant is significantly smaller than one Jupiter mass, which is valid by the definition of a gas giant.

C. W. Ormel & H. H. Klahr 2010). This channel requires the preexistence of a massive seed with significant gravity to kickstart and sustain the process. The rate of pebble accretion depends on the disk gas properties so we first introduce the disk surface density Σ_{gas} and the temperature profiles we adopt. For our fiducial surface density, we adopt the minimum mass extrasolar nebula reported by E. Chiang & G. Laughlin (2013):

$$\Sigma_{\text{gas}} = 1.3 \times 10^{-5} \left(\frac{a}{0.2 \text{ AU}} \right)^{-1.6} \text{ g cm}^{-2}, \quad (2)$$

and for our radial temperature profile, we use

$$T = 150 \text{ K} \left(\frac{a}{1 \text{ AU}} \right)^{-3/7} \quad (3)$$

from E. I. Chiang & P. Goldreich (1997) for a passive disk.

Since the solid accretion occurs onto an already formed Jupiter, pebble accretion is always in the shear regime such that

$$\dot{M}_{\text{peb}} = \Sigma \Omega \left[\sqrt{2} R_{\text{Hill}} St^{1/3} \right]^2, \quad (4)$$

where $R_{\text{Hill}} \equiv a (M_p/3M_\star)^{1/3}$ is the Hill radius, $St \equiv t_{\text{stop}} \Omega$ is the Stokes number, and t_{stop} is the aerodynamic stopping time. We parametrize the size of the particles by varying St from 0.0001 to 0.01 and verify that in all the cases, our accreting planet remains in the shear-dominated regime.

Finally, we consider pollution by migration. For a planet moving radially at speed \dot{a} , we can write the rate of mass accretion as

$$\dot{M}_{\text{mig}} = 2\pi \dot{a} \Sigma R_p, \quad (5)$$

where we assume all the material that directly hit the planet as the latter migrates undergo inelastic collision.

As the orbiting planet tidally perturbs the gas, the gas torques back on the planet. Any non-zero net torque will cause the planet to migrate inwards or outward, depending on the sign of the net torque. The exact behavior (both the direction and the magnitude) of the migration depends very sensitively on the disk structure, including its turbulent and radiative properties (e.g., S. Paardekooper et al. 2023). Here, we adopt Type I migration modified for gap opening presented by K. D. Kanagawa et al. (2018) which likely places an upper limit on the pollution rate by migration. The torque τ is related to the orbital angular momentum of the planet L via

$$\tau = \frac{\partial L}{\partial a} \dot{a} = \left(\frac{M_p \Omega a}{2} \right) \dot{a}. \quad (6)$$

Meanwhile, the net torque from planet-disk interaction is (e.g., W. Kley & R. Nelson 2012)

$$\tau = - \frac{G^2 M_p^2 \Sigma_{\text{gap}}}{c_s^2} \frac{H}{H} H, \quad (7)$$

where $c_s \equiv (kT/\mu m_H)^{1/2}$ is the sound speed, $\mu \equiv 2.7$ is the mean molecular weight, $H \equiv c_s/\Omega$ is the disk scale height, and Σ_{gap} is the surface density within the gap carved out by the planet,

$$\Sigma_{\text{gap}} \equiv \frac{\Sigma_{\text{gas}}}{1 + 0.034K}, \quad (8)$$

where

$$K \equiv \left(\frac{H}{a} \right)^{-5} \left(\frac{M_p}{M_\star} \right)^2 \alpha^{-1} \quad (9)$$

with $\alpha = 10^{-3}$, the Shakura-Sunyaev turbulent alpha.⁷ In writing equation 7, we ignored order unity numerical coefficient (~ 2.5 for our choice of Σ_{gas} and T). We discuss below in Section 3 how accounting for this coefficient would not change our final result. Planets were initially placed between 0.5 and 50 AU and we evolve their inward migration by integrating equation 6.

We further account for the dissipation of the disk gas using

$$\Sigma_{\text{gas}}(t) = f_{\text{dep}} \Sigma_{\text{gas},0} e^{t/t_{\text{disk}}}, \quad (10)$$

where $\Sigma_{\text{gas},0}$ is set by equation 2, f_{dep} is a depletion factor we vary between 0.001 and 1, and $t_{\text{disk}} = 2$ Myr is the disk lifetime (e.g., E. E. Mamajek 2009).⁸

2.2. Solid Disk Density Profiles

We now establish the solid disk surface density profile Σ . Under the minimum mass extrasolar nebula (MMEN) constructed by F. Dai et al. (2020),

$$\Sigma = \Sigma_0 \left(\frac{a}{\text{AU}} \right)^{-1.76} \quad (11)$$

where $\Sigma_0 = 50 \text{ g cm}^{-2}$ which is very close to, but nevertheless an update of the result of E. Chiang & G. Laughlin (2013).

There is a significant scatter in the normalization of MMEN ($50_{-20}^{+33} \text{ g cm}^{-2}$) due to the scatter in the exoplanet radius/mass measurements. Likewise, there are

⁷ While the α is constrained to be low in the outer regions of the disk ($\lesssim 10^{-4}$; e.g., C. Pinte et al. 2015, K. M. Flaherty et al. 2017, E. J. Lee 2024), it is unclear whether α would stay as low at short orbital periods that are relevant to Ariel.

⁸ While the more improved disk lifetime is closer to ~ 7 –8 Myr (e.g., A. Michel et al. 2021), Jupiters are more likely to appear around more massive stars which tend to have shorter-lived disks (e.g., Á. Ribas et al. 2015) so we use 2 Myr as our nominal value.

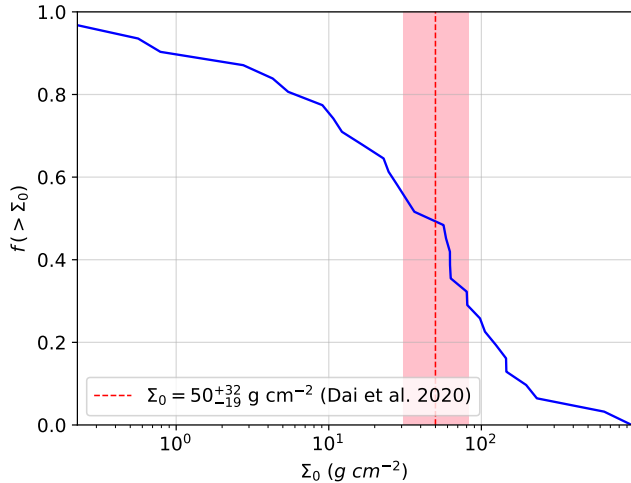


Figure 1. Cumulative distribution function of solid disk densities at 1 AU (Σ_0) calculated from protoplanetary disks in C. F. Manara et al. (2023) around stars of mass $\geq 1M_\odot$.

orders of magnitude scatter in the measured dust masses in protoplanetary disks, both in more evolved T Tauri phases (e.g., C. F. Manara et al. 2023) and in young Class 0/I phases (e.g., J. J. Tobin et al. 2020). To account for this inter-system variation, we draw Σ_0 from the dust masses reported in C. F. Manara et al. (2023), multiplied by a factor of 3 to obtain the initial solid mass (this multiplicative adjustment brings the T Tauri disk mass into agreement with that of Class 0/I; see, e.g., Y. Chachan & E. J. Lee 2023). The normalization of Σ anchored to 1 AU was derived by assuming the disk follows $\Sigma \propto a^{-1.76}$ from 0.1 to 100 AU. Figure 1 illustrates the cumulative distribution function of Σ_0 . We see that the result of F. Dai et al. (2020) corresponds to $\sim 50^{\text{th}}$ percentile, consistent with the idea that MMEN represents a *typical* disk that eventually forms exoplanetary systems. We note that only the dust masses around stars more massive than $1 M_\odot$ are chosen for this exercise given that giants are more common around such stars (e.g., A. Cumming et al. 2008; B. J. Fulton et al. 2021).

Under in situ planetesimal and pebble accretion, we account for the corresponding reduction in Σ following

$$\dot{\Sigma} = -\frac{\dot{M}}{2\pi a \delta a} \quad (12)$$

where \dot{M} is the mass accretion rate of the planet as described in Section 2.1 and δa is the width of the feeding zone. Following the arguments outlined in Section 2.1,

$$\delta a|_{\text{pla}} = R_p \quad (13)$$

for planetesimal accretion, and

$$\delta a|_{\text{peb}} = \sqrt{2} a S t^{1/3} \left(\frac{M_p}{3M_\odot} \right)^{1/3} \quad (14)$$

for pebble accretion. Both \dot{M} and $\dot{\Sigma}$ are solved simultaneously using the forward Euler method up to 1 and 10 Myr using 32 000 and 320 000 linearly spaced timesteps respectively. Integration is stopped prematurely if the total amount of solid remaining is less than that of a single planetesimal/pebble: a planetesimal is taken to be $4 \times 10^{12} \text{g}$ and have a 10 km diameter while a pebble is taken to be $4 \times 10^{-6} \text{g}$ and 1 cm across. Under migration, we do not evolve Σ but simply stop the planet migration and accretion at 10 Myr or when the planet reaches 10 days—which is the typical expected disk truncation edge under magnetospheric truncation (see, e.g., E. J. Lee & E. Chiang 2017; K. Batygin et al. 2023)—whichever comes first.

2.2.1. Dust Replenishment

Our model setup implicitly treats the planet feeding zone to be isolated (i.e., no replenishment of solids). For planetesimal accretion, unless there are neighboring planets that can systematically scatter the planetesimals in, there is no a priori reason why a given feeding zone would be replenished. For pebble accretion, the picture is more complicated as the pebbles drift in aerodynamically and the drift timescale is shorter than pebble accretion time by factors of up to ~ 10 (e.g., J. W. Lin et al. 2018; Y. Chachan & E. J. Lee 2023). One way to stop this radial drift-in is to establish a pressure trap (e.g., P. Pinilla et al. 2012). While the exact source of the pressure trap remains debated—the most popular being perturbation by an embedded planet—it is a natural mechanism to explain both the longevity of dust disks and the observed concentric ring-like structures in protoplanetary disks (see, e.g., J. Bae et al. 2023, for a review).

The efficiency with which the dust remains trapped in these pressure bumps has recently been called into question. Early analytic and numerical simulations found the traps to be imperfect only for particles of sufficiently small Stokes number which can be readily filtered through (e.g., Z. Zhu et al. 2012). More recent 2D local shearing box (e.g., E. J. Lee et al. 2022) and 3D global disk simulations (e.g., P. Huang et al. 2025) report the traps to be leaky even for Stokes number as large as 0.1 when the traps are established by an embedded planet, with the traps becoming more leaky for a lighter planet and larger turbulent diffusion coefficient. Such numerical findings are consistent with recent observations that find the abundance of volatiles in the inner disk to be largely unaffected by the presence of outer substructures (e.g., G. Perotti et al. 2023; D. Gasman et al. 2025).

Given the range of possibilities, we explore the two limiting cases. Our isolated in situ pebble accretion cor-

responds to the case of a perfect trap created by the accreting Jupiter. We introduce another limiting case of a trap that is so inefficient that the trap is functionally non-existent. In this latter case, the planet has access to all the initial dust material exterior to its orbit:

$$M_{\text{dust}}(> a_{\text{pl}}) \equiv 2\pi \int_{a_{\text{pl}}/\text{AU}}^{100} \Sigma_0 \left(\frac{a}{\text{AU}} \right)^{-0.76} d \left(\frac{a}{\text{AU}} \right) \quad (15)$$

where a_{pl} is the orbital distance of the accreting planet. We compute the amount of solids accreted onto the planet by multiplying $M_{\text{dust}}(> a_{\text{pl}})$ by $\epsilon = 0.1$ where ϵ is the pebble accretion efficiency defined as the ratio of the pebble accretion rate to the radial drift rate (see Y. Chachan & E. J. Lee 2023, for detail).

2.2.2. Water Abundance

So far, we have computed the total mass of the metals that would be accreted onto a giant planet through post-formation pollution. Creating a large uniform sample of atmospheric measurements is most amenable for volatile species such as water which is more easily detectable than tracers of refractory species such as sulfur or nitrogen. Treatment of water abundance depends on the location at which the solids were accreted. Inside the iceline, water is in gaseous form, so post-formation accretion of solids would not impact water abundance, hence the water abundance is set by the initial solar value, which we take as 0.48 (oxygen mass fraction among all metals; N. Grevesse & A. Noels 1993) times 0.02 (our adopted solar metallicity), irrespective of pollution parameters. Outside the iceline, water is in solid form, so we estimate the water abundance by multiplying the total accreted metal mass by 0.48, assuming all the oxygen to be incorporated into water for simplicity (see, e.g., K. Heng et al. 2016, their Figure 3, “cold” case). We take the water iceline at 160 K which is ~ 0.86 AU (~ 291 days) based on our adopted disk temperature profile (equation 3). For more direct comparison with observable, we further multiply our mass ratio by $2.3/18$ (solar metallicity gas mean molecular weight / mass of water molecule) to obtain number ratio.

3. RESULTS

The predicted trends of metallicity (accreted solid mass over Jupiter mass) following post-formation pollution by planetesimal accretion, pebble accretion, and disk-induced migration are found in Figures 2, 3, and 4 respectively. The abundances shown in these figures represent what is added to the planet after formation; therefore, they do not represent the absolute atmospheric abundances—in order to obtain the absolute abundances, our results would have to be added

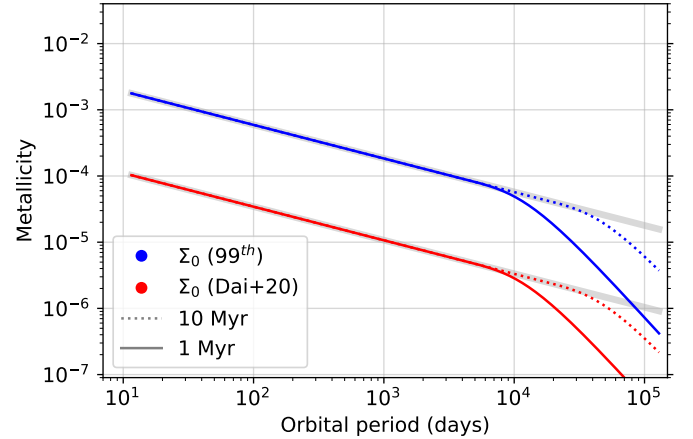


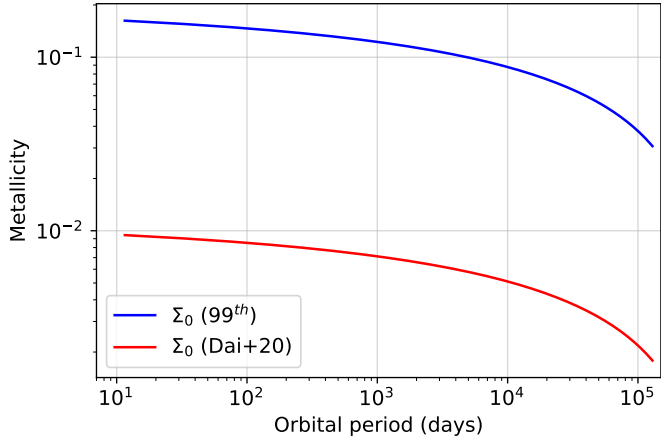
Figure 2. Predicted trend of metallicity with orbital period under local planetesimal accretion. The blue lines corresponds to highest Σ_0 (99th percentile) while the red lines illustrate Σ_0 of F. Dai et al. (2020). Solid lines show 1 Myr evolution while dotted lines show 10 Myr evolution. The gray lines signify the total available mass budget within the feeding zone.

to the metallicities the planets inherited at formation from the disk, which we assume to be stellar for simplicity. The implication is that any additive metallicity that falls below the stellar value (fixed to be 0.02 for simplicity) would simply not show up in observations as a signature of pollution. We can therefore rule out all pollution methods except pebble accretion with high Σ_0 and high $St \sim 0.01$ to be interesting.

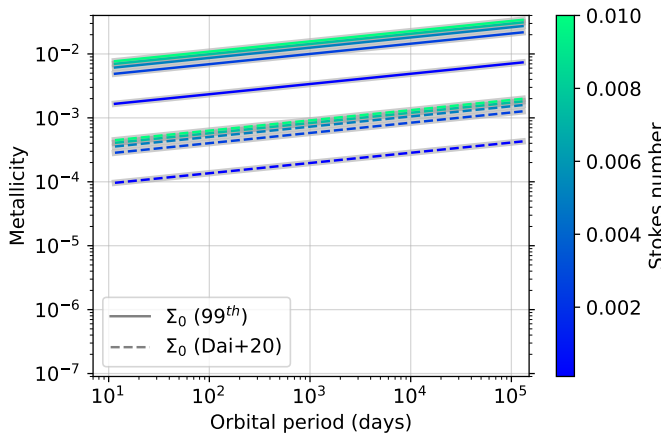
Our calculation shows that the metallicity-period trend behaves in a different manner between pebble accretion with and without dust traps with the former declining and the latter rising with orbital period. In the absence of a functional dust trap, a gas giant has access to all the solid material exterior to the planet’s orbit. Since we place a hard limit on the size of the disk at 100 AU, if the planet is located farther away from the star, there will be less mass available exterior to it. In the case where a perfect dust trap is established, a giant has access to material only within its feeding zone whose area is $2\pi a \delta a$ and the total mass within this annulus under pebble accretion is

$$M_{\text{peb}} \sim \Sigma_0 \left(\frac{a}{1 \text{ AU}} \right)^{-1.76} 2\pi a \left[\sqrt{2} a St^{1/3} \left(\frac{M_{\text{pl}}}{3M_{\odot}} \right)^{1/3} \right] \propto a^{0.24}, \quad (16)$$

which rises at larger orbital distances. The above equation also shows how M_{peb} rises with larger St . Conceptually, pebble accretion is more efficient at larger St because aerodynamic drag more easily saps away the



(a) No trapping of dust



(b) Perfect trapping of dust

Figure 3. Same as Figure 2 but for pebble accretion. The top panel corresponds to no dust trapping while the bottom panel corresponds to perfect dust traps (i.e., local accretion) where different colors correspond to varying Stokes number.

momentum of particles of larger St (as long as $St < 1$), aiding their gravitational settling onto the planet.

We discuss the metallicity-period trend of planetesimal and disk-induced migration for completeness. Local planetesimal accretion predicts a decline in the level of pollution at wider orbital separations. Repeating the calculation of M_{peb} but under planetesimal accretion whose annular area of feeding zone is $2\pi a R_p$,

$$M_{\text{pla}} = \Sigma_0 \left(\frac{a}{1 \text{ AU}} \right)^{-1.76} 2\pi a R_p \propto a^{-0.76} \quad (17)$$

which drops with orbital distance. In other words, the key difference is that in planetesimal accretion the planet's accretion cross section stays fixed, whereas in local pebble accretion the accretion cross section is bigger farther from the star.

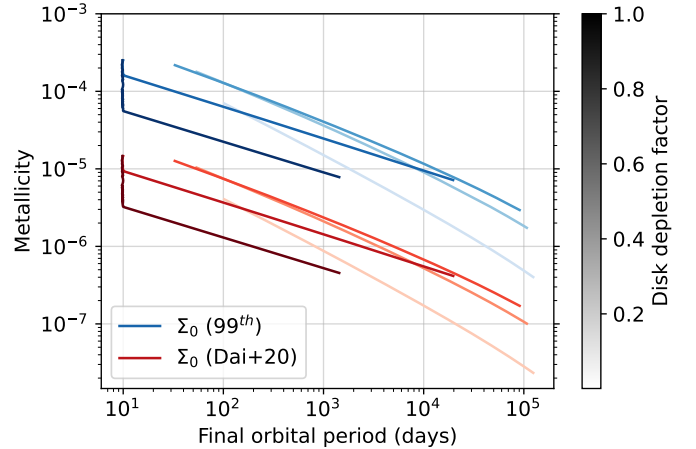


Figure 4. Predicted atmospheric metallicity under pollution by disk-induced migration with respect to the final orbital period of planets. Blue lines correspond to massive disks with Σ_0 at the 99th percentile while red lines correspond to that of typical MMEN (F. Dai et al. 2020). Varying levels of transparency correspond to f_{dep} with 1 being no gas depletion. Planets are halted either after 10 Myr or once they reach 10 days which we set to be the inner edge of the protoplanetary disk. Even the highest metallicity falls below the assumed stellar value 0.02 by roughly two orders of magnitude, much more than the order unity numerical coefficient we ignored in the torque calculation.

Likewise, under disk-induced migration, metallicity declines with the final orbital period. By definition, if the final orbital period is long, there has been minimal radial migration and the planet spends most time where Σ is lower, leading to overall lower metallicity by pollution. Figure 4 shows that the behavior of metallicity with respect to f_{dep} (gas disk depletion factor) is non-monotonic. While the total amount of metals accreted for planets migrating in gas-full ($f_{\text{dep}} = 1$) disks is larger, these planets also migrate the fastest and reach the shortest final orbital period, causing an overall leftward shift in the metallicity-final-period diagram (e.g., planets that initially start at $\sim 10^5$ days with the lowest metallicity park at $\sim 10^3$ days) with the planets that attain highest metallicity all pile up at the inner edge of 10 days.

4. SIMULATED ARIEL TRANSIT SURVEY

Our aim is to test whether any trends in water abundance with respect to orbital periods that emerge from post-formation pollution can be discerned with an Ariel survey of exoplanet atmospheres. In Figure 5, we illustrate the expected trend of total water abundance with respect to orbital period under pebble accretion, focusing on the two models where pollution is expected to achieve superstellar metallicity. In this section, we will

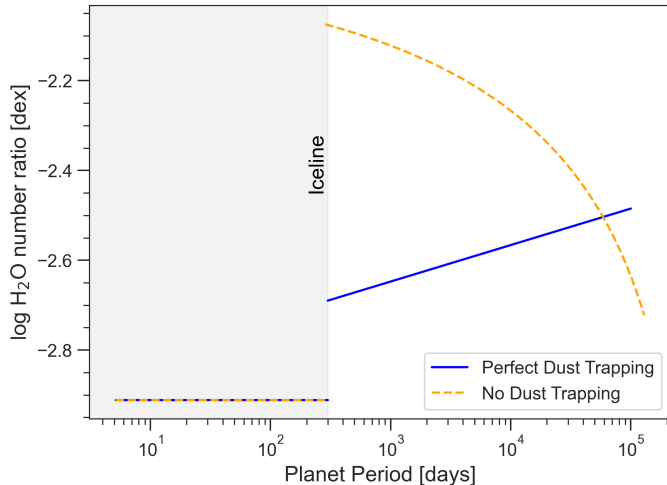


Figure 5. Predicted trend of total water abundance (number ratio) vs. orbital period. The blue line corresponds to pebble accretion with perfect dust trap with Stokes number = 0.01 and the highest Σ_0 whereas the yellow line corresponds to pebble accretion with no dust trap at the highest Σ_0 . In both cases, a discontinuity appears at our adopted iceline since inside the iceline, solid pollution does not bring additional water and the total atmospheric water content is that of stellar value.

use the model-derived water abundance shown in Figure 5 to a) quantify how well the atmospheric abundance of a planet could be constrained by Ariel Tier 2 transit spectra, and b) assess whether population-level trends in atmospheric abundance among giant planets can be used to distinguish between different origin channels of hot Jupiters.

4.1. Accuracy and Precision of Tier 2 Transit Spectroscopy Retrievals

Q. Changeat & K. H. Yip (2023) simulated Ariel retrievals for Tier 2 transmission spectra, providing estimates of how accurately and precisely water abundance could be measured with such observations. Specifically, atmospheric retrievals were done using *Alfnoor* (Q. Changeat et al. 2020) for 21,988 targets, resulting in tables of ground truths and retrieved water abundances, including 16th, 50th and 84th percentiles for each target. The median of the retrieval is simply the 50th percentile, while the 1σ confidence interval runs from the 16th to the 84th percentile and the 1σ uncertainty is half of that range. An additional cut is performed to only include planets greater than 0.3 Jupiter masses (M_{jup}), leaving 6,149 targets. Using this sample, we find that for planets with water number ratio > -5 dex, the expected uncertainty on retrievals from Tier 2 Ariel transmission spectra is 0.10 ± 0.07 dex.

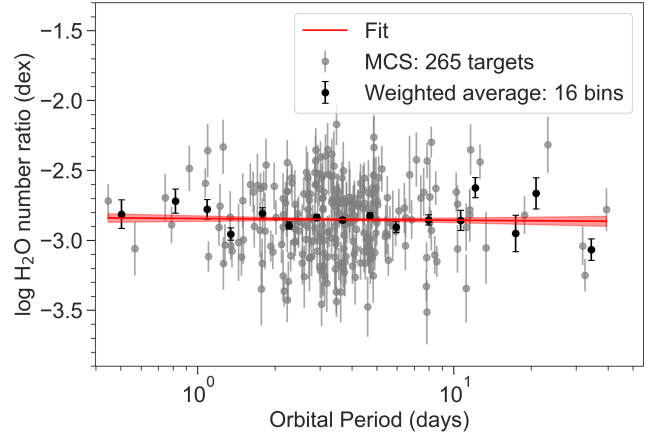


Figure 6. Measured water abundance from simulated Ariel retrievals vs orbital period using targets from the MCS under pebble accretion. The uncertainties on the retrieved water abundance, shown here in gray, are drawn from Q. Changeat & K. H. Yip (2023) as described in the text. The transit targets represent the 265 easiest-to-observe Jupiters ($M > 0.3M_{\text{jup}}$) that can be observed to Tier 2 signal-to-noise ratio in a cumulative observing time of one year. The binned data are shown in black, but the fit shown in red is determined from the unbinned data. The uncertainty on the linear fit is shown by fainter red shading. All targets are within the iceline so a flat H_2O abundance with orbital period is expected and obtained regardless of dust trapping.

To simulate Ariel observations using real targets, we use the July 2024 version of the *Ariel Mission Candidate Sample* (MCS) presented by B. Edwards & G. Tinetti (2022) and available on GitHub. We use the optimistic version of the MCS, which includes both confirmed and candidate planets. We conservatively adopt the easiest targets observable in a cumulative observing time of 1 year, where we assume that each transit observation takes $3\times$ the transit duration and each target is re-observed until it reaches Tier 2 signal-to-noise. Our mock survey includes 265 Jupiters.

Ariel’s targets are hot and warm Jupiters around FGK and early M type dwarfs so they are all within the iceline. In the simplest baseline scenario of minimal migration after pollution, we expect the water abundance to be flat with respect to orbital period set to the stellar value irrespective of the existence/efficiency of a dust trap, as shown in Figure 5. We initially assign this stellar water abundance to each planet (adding stellar $[\text{Fe}/\text{H}]$ to the solar value we adopt) and then randomly shift the abundance by 0.10 ± 0.07 dex. Figure 6 depicts simulated Ariel retrievals of 265 Tier 2 transmission spectroscopy targets after 1 year of cumulative observation time with Ariel. A fit through all the planets (i.e., raw data without binning) recovers the expected flat H_2O abundance with respect to orbital period.

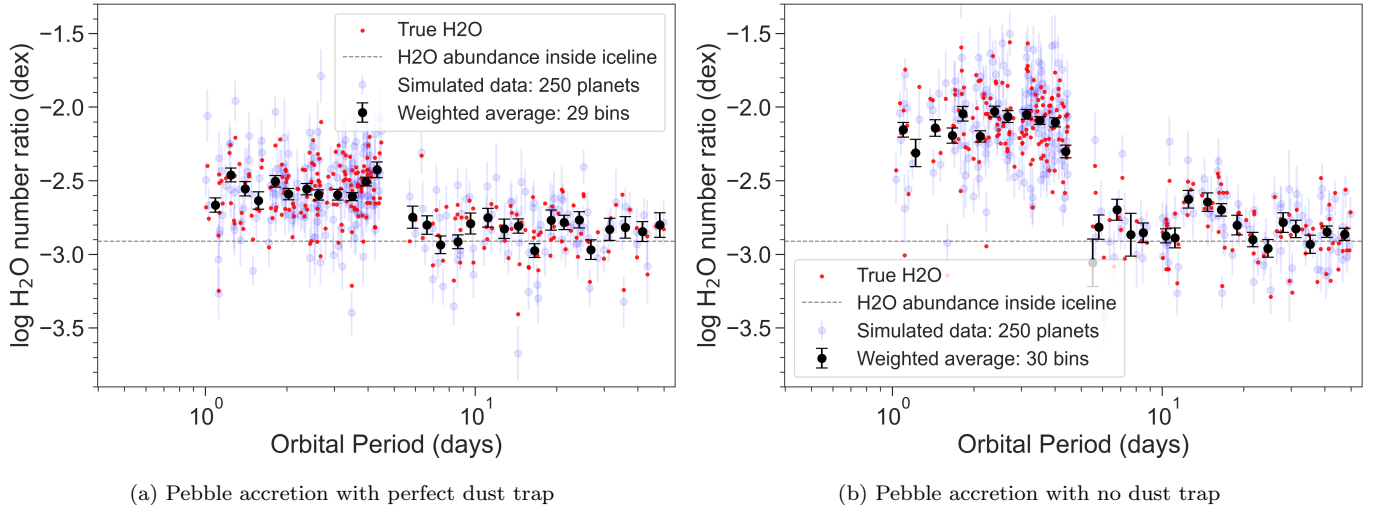


Figure 7. Measured water abundance from simulated Ariel retrievals vs. orbital period using generated planet data under pebble accretion with perfect dust traps (left) and without a dust trap (right), assuming high-eccentricity migration occurs for Jupiter-mass exoplanets that were originally at $a > 1$ AU. The red points are the assigned true water abundance whereas the blue points are the simulated data accounting for uncertainties. Black points are the weighted average of the simulated data. High-eccentricity migration predicts hot Jupiters to appear significantly more water-enriched than warm Jupiters and the amount of such an excess is expected to be detectable by Ariel.

4.2. Disk-Induced vs. High-Eccentricity Migration

Under high-eccentricity migration, a gas giant first completes its formation at large orbital separations (beyond the iceline). After the disk dissipates, the giant is excited to a highly eccentric orbit by neighboring planetary or stellar perturbers, then tidally circularizes to a tight orbit with orbital period less than ~ 10 days. Under all circumstances, giants that complete their pollution beyond the iceline are expected to have a significantly water-enriched envelope as compared to those that remain inside the iceline (because solid pollution adds extra water only beyond the iceline). We therefore expect the signature of high-eccentricity migration to show up as a sudden jump in water abundance ratio for hot Jupiters compared to warm Jupiters—insofar as most warm Jupiters did not undergo similar dynamical upheaval (e.g., M. Rice et al. 2022b; X.-Y. Wang et al. 2024).⁹

Our goal is to assess the ability of Ariel survey at the Tier 2 level to discern the aforementioned effect of high-eccentricity migration on the measurable water abundance of hot Jupiters. To simulate the migration of a giant from beyond to inside the iceline, we simply move the planets from beyond 1 AU down to ~ 1 –4 days where

we observe hot Jupiters. We generate 250 fictitious exoplanets, as this is roughly the number of Tier 2 transmission spectroscopy targets that Ariel could observe within a year. These mock planets have arbitrary initial orbital distances between 0.08 and 10 AU (for stellar masses drawn uniformly between 0.4 and $3 M_{\odot}$ encompassing 97.6% of the Jovian hosts in the MCS), water abundance set by model expectation in Figure 5 corrected to non-solar abundance drawing from the stellar [Fe/H] distribution in the MCS sample, as well as uncertainties drawn from Q. Changeat & K. H. Yip (2023) set to 0.10 ± 0.07 dex. The 10 AU upper limit to the orbital distance is motivated by the observed peak of gas giant occurrence rate at 1–10 AU (B. J. Fulton et al. 2021).

Figure 7 illustrates the resulting water abundance of hot vs. warm Jupiters. As expected, polluted hot Jupiters that undergo high-eccentricity migration from beyond the iceline are expected to be significantly more water-enriched than warm Jupiters at ~ 0.5 –1.0 dex level, which is enough to be detectable by Ariel, and visible by eye when the data are binned. The scenario with no dust traps predicts the hot Jupiters to be noticeably more water-rich than those with perfect dust traps simply because they have access to more solids (see Figure 5). Much of the scatter in true H_2O value for hot Jupiters comes from our random distribution of the initial orbital distance without any correlation to the final location in addition to the scatter in stellar metallicity. While a more detailed orbital evolution may beget

⁹ For the purposes of the simulation, we assume that the migrating Jovian planets have already reached an orbital period on the order of days. Additionally, we assume that the metallicity of the planet remains constant throughout the high-eccentricity migration.

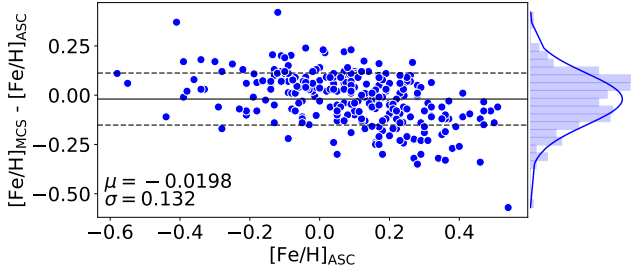


Figure 8. Metallicity comparisons from cross-matched planets in the *Mission Candidate Sample* catalogue (MCS; B. Edwards & G. Tinetti 2022) and the Ariel Stellar Characterisation working group’s catalogue (ASC; C. Danielski et al. 2022).

further trends with e.g., orbital period among the hot Jupiters, we defer such studies to future investigation.

5. DISCUSSION

5.1. Stellar Metallicity

The stellar metallicity recorded in MCS draws from the available literature and the NASA Exoplanet Archive, which can be inaccurate. A homogeneous abundance retrieval of ~ 350 host stars from a subset of potential Ariel targets has been performed by the Ariel Stellar Characterisation (ASC) working group (M. Tsantaki et al. 2025; see also C. Danielski et al. 2022 for the earlier version). We now check how much the errors in stellar metallicity could impact Ariel’s ability to discern the effect of high-eccentricity migration.

There are 270 host stars with reported metallicities that overlap between ASC (M. Tsantaki et al. 2025) and MCS (B. Edwards & G. Tinetti 2022). For these stars, we plot in Figure 8 how much the reported metallicities differ. At subsolar $[\text{Fe}/\text{H}]$ from ASC, MCS metallicities are systematically larger while at supersolar $[\text{Fe}/\text{H}]$ from ASC, MCS metallicities are systematically smaller. Such a trend suggests the MCS incorrectly attributes near-solar metallicity to many stars, under-predicting the scatter in measurable H_2O abundance in e.g., Figure 7. The $1\text{-}\sigma$ error that would be introduced by more accurate association of stellar metallicity is 0.132 dex, whose full width ($\pm 1\text{-}\sigma$) is smaller than the target signature of high-eccentricity migration 0.5–1.0 dex. We therefore conclude that the Ariel Tier 2 transit survey remains a viable method of testing the origin theory of hot Jupiters although more accurate measurements of stellar metallicities would be critical to improve both the accuracy at which polluted planets can be identified and the precision to which atmospheric trends can be recovered.

5.2. Formation Condition of Hot Jupiters

Our results suggest that for post-formation pollution to achieve superstellar atmospheric metallicity (required for observability), the mechanism of pollution must be pebble accretion, the underlying solid disk must be metal-heavy, and in case of perfect dust trap, the Stokes number of pebbles should be $\gtrsim 0.01$. The need for metal-heavy disk is consistent with the nucleation of gas giants requiring massive rocky core and the observed correlation between giants and stellar metallicity (e.g., D. A. Fischer & J. Valenti 2005). Pollution by pebble accretion implies that the pollution must occur when the disk gas remains while high Stokes number may correspond to either a reduction in disk gas density—consistent with *post*-formation pollution—or larger dust grains. We favor the former explanation based on recent analysis of young protoplanetary disks. By analyzing the shape and the mass content of ringed disks with dust equation of motion, E. J. Lee (2024) find most ringed protoplanetary disks to feature low Stokes number $\sim 10^{-4}$ – 10^{-3} . Focusing on IM Lup disk and using detailed disk models, T. Ueda et al. (2024) report that self-consistently explaining multiwavelength observations requires dust grains to be fragile corresponding to similarly low Stokes number.

5.3. Suggestion for Ariel

Under a uniform period distribution simulating 250 planets, separated into 29 period bins, we find that Ariel observations at the Tier 2 level of uncertainties are sufficient to test the effect of high-eccentricity migration of hot Jupiters by way of their elevated water abundance ratio compared to warm Jupiters (Figure 7). Even in the relatively pessimistic scenario (perfect dust trap; left panel), the simulated 250 planets having ~ 8 data points within each bin appear more than enough to beat down the stochastic noise and extract the ~ 0.5 dex difference in H_2O abundance ratio between hot and warm Jupiters at $>1\text{-}\sigma$. We therefore suggest having at minimum 100 targets to test the effect of high-eccentricity migration of hot Jupiters in comparison to warm Jupiters.

Potentially, a bigger challenge is to sample enough hot *and* warm Jupiters. Figure 6 shows that Tier 2 MCS sample we use is highly concentrated around ~ 2 –5 days of orbital period. Although this orbital period corresponds to the peak of the orbital period distribution of hot Jupiters, the distribution extends to ~ 10 days (e.g., A. Santerne et al. 2016; S. W. Yee & J. N. Winn 2023).¹⁰

¹⁰ While Figure 7 shows a clear jump in water abundance at ~ 4 days, the location of the jump is arbitrary as it is completely set by our choice of transporting planets down to 1–4 days to simulate high-eccentricity migration. It is therefore important

Based on our filtered MCS, we find that the number of warm Jupiters (orbital periods >10 days) for which we can obtain Tier 2 spectra within the first 100 days is only 7. This number increases to 11 within the first 150 days (6 inside 15 days, 5 beyond) and to 16 within a full year (all additional 5 targets with orbital periods inside 15 days). This number is more than sufficient to reach the target precision to distinguish between hot and warm Jupiter water abundance under high-eccentricity migration of the former if we group all warm Jupiters under one period bin; it is marginally sufficient if we group warm Jupiters over two period bins, separated at ~ 15 days.

The list of discovered (and confirmed) warm Jupiters by the Transiting Exoplanet Survey Satellite (TESS) continues to grow, so we expect that by the time Ariel launches, there should be enough known warm Jupiters to more definitively test the origin of hot Jupiters, making more viable a formal adoption of the orbital period as one of the axes of diversity in selecting Ariel targets (e.g., [N. B. Cowan & B. Coull-Neveu 2025](#)). We therefore suggest attention be given to quantify the likelihood of obtaining Tier 2 level spectra of this growing list of confirmed Jovians beyond 10 day orbital period.

While a hierarchical model fit (e.g., [D. Keating & N. B. Cowan 2022](#)) could improve precision, we consider it unnecessary for the test of high-eccentricity migration. A more critical requirement is to build a target list that has enough representation of *both* hot and warm Jupiters (but not necessarily equal representation) for which deep survey (Tier 2) Ariel spectra can be obtained. Another critical observational effort in this regard is to develop an accurate and uniform set of host star metallicities (e.g., [C. Danielski et al. 2022](#); [M. Tsantaki et al. 2025](#)) to first determine whether a given planet has superstellar metallicities which would be a criterion one can use to identify candidate planets that underwent post-formation pollution.

5.4. Connection to Cold Jupiters

Our discussion thus far focused on using the difference in hot Jupiter’s water abundance with respect to warm Jupiters under high-eccentricity migration. In our simple baseline scenario of warm Jupiters barely undergoing any post-formation migration, we do not expect to find any trend in water abundance with respect to orbital period among the warm Jupiters. A trend

appears only beyond the iceline and [Figure 5](#) demonstrates how the behavior of such a trend differs significantly between the case with and without functioning dust traps. While directly resolving the full trend is not possible with current technology, one may compare the hot Jupiter’s water abundance ratio from e.g., Ariel with that of directly imaged planets from e.g., James Webb Space Telescope (JWST). Under high-eccentricity migration, hot Jupiters would originate from 1–10 AU ($\sim 365\text{--}10^4$ days) while directly imaged planets would be beyond ~ 10 s of AU. If there was effectively no dust trapping, we expect hot Jupiters to be more water-enriched than wide-orbit planets. If on the other hand there was a perfect dust trap, we expect the opposite. Systematic comparison of atmospheric abundances between hot and cold Jupiters therefore can be used as a test of the efficiencies of dust traps in protoplanetary disks that nucleate gas giants. Such studies would likely require calibrating abundance measurements from transit, emission and reflectance spectroscopy, since the short-period and long-period planets would have to be characterized via different techniques.

6. CONCLUSION

We explored three post-formation pollution mechanisms—planetesimal accretion, pebble accretion, and disk-induced migration—to construct a theoretical prediction of gas giants’ atmospheric water abundance as a function of orbital period. Only pebble accretion in highly metal-heavy disks is able to achieve supersolar metallicity in giant planet atmosphere leaving a detectable signature of pollution. If the dominant origin channel of hot Jupiters is high-eccentricity migration while that of warm Jupiters is more dynamically quiescent, we expect a significant upward shift in their atmospheric water abundance compared to warm Jupiters, at a level that is detectable with Ariel. To ensure that it can constrain these formation/migration scenarios, the Ariel Tier 2 transit survey should include $\mathcal{O}(100)$ hot (<10 days) *and* warm (>10 days) Jupiters with at least $\sim 8\text{--}16$ warm Jupiters beyond 10 days. We further suggest a comparison of median hot Jupiter water abundance with that of wide-orbit cold Jupiters which can be leveraged to reveal the property of primordial protoplanetary disks such as the existence and the efficacy of the dust trap established by the embedded giant planet(s).

ACKNOWLEDGMENTS

We thank Quentin Changeat for clarifying discussion on Ariel uncertainties. We also thank Quinn Konopacky,

to use an independent definition of hot vs. warm Jupiters which are usually divided into those at orbital periods less than and greater than 10 days based on occurrence rate studies (e.g., [A. Santerne et al. 2016](#); [S. W. Yee & J. N. Winn 2023](#)).

Jean-Baptiste Ruffio, and Jason Wang for useful discussions on atmospheric characterization of directly imaged planets. LD was supported by the Trottier internship from the Trottier Institute for Research on Exoplanets. BCN gratefully acknowledges support by the Trottier Space Institute and McGill University. EJL gratefully acknowledges support by NSERC, by FRQNT, by the Trottier Space Institute, and by the William Dawson Scholarship from McGill University. NBC acknowledges

support from a Canada Research Chair, NSERC Discovery Grant, and McDonald Fellowship.

AUTHOR CONTRIBUTIONS

LD performed the theoretical modelling of expected metallicities. BCN carried out modelling of observational expectations of Ariel. EJL conceived the research concept and supervised the overall project. NBC supervised BCN and provided observational and data analysis expertise.

REFERENCES

- Antonini, F., Hamers, A. S., & Lithwick, Y. 2016, *AJ*, 152, 174, doi: [10.3847/0004-6256/152/6/174](https://doi.org/10.3847/0004-6256/152/6/174)
- Bae, J., Isella, A., Zhu, Z., et al. 2023, in *Astronomical Society of the Pacific Conference Series*, Vol. 534, *Protostars and Planets VII*, ed. S. Inutsuka, Y. Aikawa, T. Muto, K. Tomida, & M. Tamura, 423, doi: [10.48550/arXiv.2210.13314](https://doi.org/10.48550/arXiv.2210.13314)
- Barstow, J. K., Changeat, Q., Chubb, K. L., et al. 2022, *Experimental Astronomy*, 53, 447, doi: [10.1007/s10686-021-09821-w](https://doi.org/10.1007/s10686-021-09821-w)
- Batygin, K., Adams, F. C., & Becker, J. 2023, *ApJL*, 951, L19, doi: [10.3847/2041-8213/acdb5d](https://doi.org/10.3847/2041-8213/acdb5d)
- Bitsch, B., Morbidelli, A., Johansen, A., et al. 2018, *A&A*, 612, A30, doi: [10.1051/0004-6361/201731931](https://doi.org/10.1051/0004-6361/201731931)
- Chachan, Y., & Lee, E. J. 2023, *ApJL*, 952, L20, doi: [10.3847/2041-8213/ace257](https://doi.org/10.3847/2041-8213/ace257)
- Changeat, Q., Al-Refaie, A., Mugnai, L. V., et al. 2020, *The Astronomical Journal*, 160, 80, doi: [10.3847/1538-3881/ab9a53](https://doi.org/10.3847/1538-3881/ab9a53)
- Changeat, Q., & Yip, K. H. 2023, *arXiv*, doi: [10.48550/arXiv.2206.14633](https://doi.org/10.48550/arXiv.2206.14633)
- Chiang, E., & Laughlin, G. 2013, *MNRAS*, 431, 3444, doi: [10.1093/mnras/stt424](https://doi.org/10.1093/mnras/stt424)
- Chiang, E. I., & Goldreich, P. 1997, *ApJ*, 490, 368, doi: [10.1086/304869](https://doi.org/10.1086/304869)
- Cowan, N. B., & Coull-Neveu, B. 2025, *arXiv e-prints*, *arXiv:2506.06429*, doi: [10.48550/arXiv.2506.06429](https://doi.org/10.48550/arXiv.2506.06429)
- Cumming, A., Butler, R. P., Marcy, G. W., et al. 2008, *PASP*, 120, 531, doi: [10.1086/588487](https://doi.org/10.1086/588487)
- Dai, F., Winn, J. N., Schlaufman, K., et al. 2020, *AJ*, 159, 247, doi: [10.3847/1538-3881/ab88b8](https://doi.org/10.3847/1538-3881/ab88b8)
- Danielski, C., Brucalassi, A., Benatti, S., et al. 2022, *Experimental Astronomy*, 53, 473, doi: [10.1007/s10686-021-09765-1](https://doi.org/10.1007/s10686-021-09765-1)
- Dawson, R. I., & Johnson, J. A. 2018, *ARA&A*, 56, 175, doi: [10.1146/annurev-astro-081817-051853](https://doi.org/10.1146/annurev-astro-081817-051853)
- Edwards, B., & Tinetti, G. 2022, *AJ*, 164, 15, doi: [10.3847/1538-3881/ac6bf9](https://doi.org/10.3847/1538-3881/ac6bf9)
- Fischer, D. A., & Valenti, J. 2005, *The Astrophysical Journal*, 622, 1102, doi: [10.1086/428383](https://doi.org/10.1086/428383)
- Flaherty, K. M., Hughes, A. M., Rose, S. C., et al. 2017, *ApJ*, 843, 150, doi: [10.3847/1538-4357/aa79f9](https://doi.org/10.3847/1538-4357/aa79f9)
- Fulton, B. J., Rosenthal, L. J., Hirsch, L. A., et al. 2021, *ApJS*, 255, 14, doi: [10.3847/1538-4365/abfcc1](https://doi.org/10.3847/1538-4365/abfcc1)
- Fung, J., & Lee, E. J. 2018, *ApJ*, 859, 126, doi: [10.3847/1538-4357/aabaf7](https://doi.org/10.3847/1538-4357/aabaf7)
- Gasman, D., Temmink, M., van Dishoeck, E. F., et al. 2025, *A&A*, 694, A147, doi: [10.1051/0004-6361/202452152](https://doi.org/10.1051/0004-6361/202452152)
- GRAVITY Collaboration, Nowak, M., Lacour, S., et al. 2020, *A&A*, 633, A110, doi: [10.1051/0004-6361/201936898](https://doi.org/10.1051/0004-6361/201936898)
- Grevesse, N., & Noels, A. 1993, in *Origin and Evolution of the Elements*, ed. N. Prantzos, E. Vangioni-Flam, & M. Casse, 15–25
- Hallatt, T., & Lee, E. J. 2020, *ApJ*, 904, 134, doi: [10.3847/1538-4357/abc1d7](https://doi.org/10.3847/1538-4357/abc1d7)
- Heng, K., Lyons, J. R., & Tsai, S.-M. 2016, *ApJ*, 816, 96, doi: [10.3847/0004-637X/816/2/96](https://doi.org/10.3847/0004-637X/816/2/96)
- Huang, C., Wu, Y., & Triaud, A. H. M. J. 2016, *ApJ*, 825, 98, doi: [10.3847/0004-637X/825/2/98](https://doi.org/10.3847/0004-637X/825/2/98)
- Huang, P., Yu, F., Lee, E. J., Dong, R., & Bai, X.-N. 2025, *arXiv e-prints*, *arXiv:2503.19026*, doi: [10.48550/arXiv.2503.19026](https://doi.org/10.48550/arXiv.2503.19026)
- Kanagawa, K. D., Tanaka, H., & Szuszkiewicz, E. 2018, *ApJ*, 861, 140, doi: [10.3847/1538-4357/aac8d9](https://doi.org/10.3847/1538-4357/aac8d9)
- Karalis, A., Lee, E. J., & Thorngren, D. P. 2025, *ApJ*, 978, 46, doi: [10.3847/1538-4357/ad946c](https://doi.org/10.3847/1538-4357/ad946c)
- Keating, D., & Cowan, N. B. 2022, *MNRAS*, 509, 289, doi: [10.1093/mnras/stab2941](https://doi.org/10.1093/mnras/stab2941)
- Kley, W., & Nelson, R. 2012, *Annual Review of Astronomy and Astrophysics*, 50, 211, doi: [10.1146/annurev-astro-081811-125523](https://doi.org/10.1146/annurev-astro-081811-125523)

- Lee, E. J. 2024, *ApJL*, 970, L15, doi: [10.3847/2041-8213/ad5d8e](https://doi.org/10.3847/2041-8213/ad5d8e)
- Lee, E. J., & Chiang, E. 2017, *ApJ*, 842, 40, doi: [10.3847/1538-4357/aa6fb3](https://doi.org/10.3847/1538-4357/aa6fb3)
- Lee, E. J., Chiang, E., & Ormel, C. W. 2014, *ApJ*, 797, 95, doi: [10.1088/0004-637X/797/2/95](https://doi.org/10.1088/0004-637X/797/2/95)
- Lee, E. J., Fuentes, J. R., & Hopkins, P. F. 2022, *ApJ*, 937, 95, doi: [10.3847/1538-4357/ac8cfe](https://doi.org/10.3847/1538-4357/ac8cfe)
- Lin, J. W., Lee, E. J., & Chiang, E. 2018, *MNRAS*, 480, 4338, doi: [10.1093/mnras/sty2159](https://doi.org/10.1093/mnras/sty2159)
- Madhusudhan, N., Amin, M. A., & Kennedy, G. M. 2014, *ApJL*, 794, L12, doi: [10.1088/2041-8205/794/1/L12](https://doi.org/10.1088/2041-8205/794/1/L12)
- Mamajek, E. E. 2009, EXOPLANETS AND DISKS: THEIR FORMATION AND DIVERSITY: Proceedings of the International Conference. AIP Conference Proceedings, 1158, 3, doi: [10.1063/1.3215910](https://doi.org/10.1063/1.3215910)
- Manara, C. F., Ansdell, M., Rosotti, G. P., et al. 2023, in *Astronomical Society of the Pacific Conference Series*, Vol. 534, Protostars and Planets VII, ed. S. Inutsuka, Y. Aikawa, T. Muto, K. Tomida, & M. Tamura, 539, doi: [10.48550/arXiv.2203.09930](https://doi.org/10.48550/arXiv.2203.09930)
- Matsakos, T., & Königl, A. 2016, *The Astrophysical Journal Letters*, 820, 0, doi: [10.3847/2041-8205/820/1/L8](https://doi.org/10.3847/2041-8205/820/1/L8)
- Michel, A., van der Marel, N., & Matthews, B. C. 2021, *ApJ*, 921, 72, doi: [10.3847/1538-4357/ac1bbb](https://doi.org/10.3847/1538-4357/ac1bbb)
- Mollière, P., Molyarova, T., Bitsch, B., et al. 2022, *ApJ*, 934, 74, doi: [10.3847/1538-4357/ac6a56](https://doi.org/10.3847/1538-4357/ac6a56)
- Mugnai, L. V., Al-Refaie, A., Bocchieri, A., et al. 2021, *AJ*, 162, 288, doi: [10.3847/1538-3881/ac2e92](https://doi.org/10.3847/1538-3881/ac2e92)
- Nasedkin, E., Mollière, P., Lacour, S., et al. 2024, *A&A*, 687, A298, doi: [10.1051/0004-6361/202449328](https://doi.org/10.1051/0004-6361/202449328)
- Öberg, K. I., Murray-Clay, R., & Bergin, E. A. 2011, *ApJL*, 743, L16, doi: [10.1088/2041-8205/743/1/L16](https://doi.org/10.1088/2041-8205/743/1/L16)
- Öberg, K. I., & Wordsworth, R. 2019, *AJ*, 158, 194, doi: [10.3847/1538-3881/ab46a8](https://doi.org/10.3847/1538-3881/ab46a8)
- Ormel, C. W., & Klahr, H. H. 2010, *Astronomy and Astrophysics*, 520, A43, doi: [10.1051/0004-6361/201014903](https://doi.org/10.1051/0004-6361/201014903)
- Owen, J. E., & Lai, D. 2018, *MNRAS*, 479, 5012, doi: [10.1093/mnras/sty1760](https://doi.org/10.1093/mnras/sty1760)
- Paardekooper, S., Dong, R., Duffell, P., et al. 2023, in *Astronomical Society of the Pacific Conference Series*, Vol. 534, Protostars and Planets VII, ed. S. Inutsuka, Y. Aikawa, T. Muto, K. Tomida, & M. Tamura, 685, doi: [10.48550/arXiv.2203.09595](https://doi.org/10.48550/arXiv.2203.09595)
- Penzlin, A. B. T., Booth, R. A., Kirk, J., et al. 2024, *MNRAS*, 535, 171, doi: [10.1093/mnras/stae2362](https://doi.org/10.1093/mnras/stae2362)
- Perotti, G., Christiaens, V., Henning, T., et al. 2023, *Nature*, 620, 516, doi: [10.1038/s41586-023-06317-9](https://doi.org/10.1038/s41586-023-06317-9)
- Petrovich, C., & Tremaine, S. 2016, *The Astrophysical Journal*, 829, 132, doi: [10.3847/0004-637X/829/2/132](https://doi.org/10.3847/0004-637X/829/2/132)
- Pinilla, P., Birnstiel, T., Ricci, L., et al. 2012, *A&A*, 538, A114, doi: [10.1051/0004-6361/201118204](https://doi.org/10.1051/0004-6361/201118204)
- Pinte, C., Dent, W. R. F., Ménard, F., et al. 2015, *The Astrophysical Journal*, 816, 25, doi: [10.3847/0004-637X/816/1/25](https://doi.org/10.3847/0004-637X/816/1/25)
- Piso, A.-M. a., Youdin, A. N., & Murray-Clay, R. a. 2015, *The Astrophysical Journal*, 800, 82, doi: [10.1088/0004-637X/800/2/82](https://doi.org/10.1088/0004-637X/800/2/82)
- Rafikov, R. R. 2006, *The Astrophysical Journal*, 648, 666, doi: [10.1086/505695](https://doi.org/10.1086/505695)
- Ribas, Á., Bouy, H., & Merín, B. 2015, *A&A*, 576, A52, doi: [10.1051/0004-6361/201424846](https://doi.org/10.1051/0004-6361/201424846)
- Rice, M., Wang, S., & Laughlin, G. 2022a, *ApJL*, 926, L17, doi: [10.3847/2041-8213/ac502d](https://doi.org/10.3847/2041-8213/ac502d)
- Rice, M., Wang, S., Wang, X.-Y., et al. 2022b, *AJ*, 164, 104, doi: [10.3847/1538-3881/ac8153](https://doi.org/10.3847/1538-3881/ac8153)
- Santerne, A., Moutou, C., Tsantaki, M., et al. 2016, *A&A*, 587, A64, doi: [10.1051/0004-6361/201527329](https://doi.org/10.1051/0004-6361/201527329)
- Savignac, V., & Lee, E. J. 2024, *ApJ*, 973, 85, doi: [10.3847/1538-4357/ad6317](https://doi.org/10.3847/1538-4357/ad6317)
- Schneider, A. D., & Bitsch, B. 2021, *A&A*, 654, A71, doi: [10.1051/0004-6361/202039640](https://doi.org/10.1051/0004-6361/202039640)
- Swain, M. R., Hasegawa, Y., Thorngren, D. P., & Roudier, G. M. 2024, *SSRv*, 220, 61, doi: [10.1007/s11214-024-01098-7](https://doi.org/10.1007/s11214-024-01098-7)
- Tinetti, G., Eccleston, P., Lueftinger, T., et al. 2022, in *European Planetary Science Congress, EPSC2022–1114*, doi: [10.5194/epsc2022-1114](https://doi.org/10.5194/epsc2022-1114)
- Tinetti, G., Drossart, P., Eccleston, P., et al. 2018, *Experimental Astronomy*, 46, 135, doi: [10.1007/s10686-018-9598-x](https://doi.org/10.1007/s10686-018-9598-x)
- Tinetti, G., Eccleston, P., Haswell, C., et al. 2021, <https://arxiv.org/abs/2104.04824>
- Tobin, J. J., Sheehan, P. D., Megeath, S. T., et al. 2020, *ApJ*, 890, 130, doi: [10.3847/1538-4357/ab6f64](https://doi.org/10.3847/1538-4357/ab6f64)
- Tsantaki, M., Magrini, L., Danielski, C., et al. 2025, *A&A*, 697, A102, doi: [10.1051/0004-6361/202453059](https://doi.org/10.1051/0004-6361/202453059)
- Turrini, D., Codella, C., Danielski, C., et al. 2022, *Experimental Astronomy*, 53, 225, doi: [10.1007/s10686-021-09754-4](https://doi.org/10.1007/s10686-021-09754-4)
- Ueda, T., Tazaki, R., Okuzumi, S., Flock, M., & Sudarshan, P. 2024, *Nature Astronomy*, 8, 1148, doi: [10.1038/s41550-024-02308-6](https://doi.org/10.1038/s41550-024-02308-6)
- Vlahos, E., Chachan, Y., Savignac, V., & Lee, E. J. 2024, *ApJ*, 976, 237, doi: [10.3847/1538-4357/ad83d5](https://doi.org/10.3847/1538-4357/ad83d5)
- Wang, X.-Y., Rice, M., Wang, S., et al. 2024, *ApJL*, 973, L21, doi: [10.3847/2041-8213/ad7469](https://doi.org/10.3847/2041-8213/ad7469)

Yee, S. W., & Winn, J. N. 2023, *ApJL*, 949, L21,
doi: [10.3847/2041-8213/acd552](https://doi.org/10.3847/2041-8213/acd552)

Zhu, Z., Nelson, R. P., Dong, R., Espaillat, C., &
Hartmann, L. 2012, *ApJ*, 755, 6,
doi: [10.1088/0004-637X/755/1/6](https://doi.org/10.1088/0004-637X/755/1/6)